

Quantitative differential phase contrast imaging in an LED array microscope

Lei Tian^{1,*} and Laura Waller²

¹Department of Electrical Engineering and Computer Sciences, University of California, Berkeley, CA, 94709, USA

*lei_tian@alum.mit.edu

Abstract: Illumination-based differential phase contrast (DPC) is a phase imaging method that uses a pair of images with asymmetric illumination patterns. Distinct from coherent techniques, DPC relies on spatially partially coherent light, providing $2\times$ better lateral resolution, better optical sectioning and immunity to speckle noise. In this paper, we derive the 2D weak object transfer function (WOTF) and develop a quantitative phase reconstruction method that is robust to noise. The effect of spatial coherence is studied experimentally, and multiple-angle DPC is shown to provide improved frequency coverage for more stable phase recovery. Our method uses an LED array microscope to achieve real-time (10 Hz) quantitative phase imaging with *in vitro* live cell samples.

© 2015 Optical Society of America

OCIS codes: (100.5070) Phase retrieval; (110.1758) Computational imaging; (170.0180) Microscopy; (110.3010) Image reconstruction techniques.

References and links

1. F. Zernike, "Phase contrast, a new method for the microscopic observation of transparent objects," *Physica* **9**, 686–698 (1942).
2. M. R. Teague, "Deterministic phase retrieval: a Green's function solution," *J. Opt. Soc. Am.* **73**, 1434–1441 (1983).
3. N. Streibl, "Phase imaging by the transport equation of intensity," *Opt. Commun.* **49**, 6–10 (1984).
4. C. J. R. Sheppard, "Defocused transfer function for a partially coherent microscope and application to phase retrieval," *J. Opt. Soc. Am. A* **21**, 828–831 (2004).
5. S. S. Kou, L. Waller, G. Barbastathis, P. Marquet, C. Depeursinge, and C. J. R. Sheppard, "Quantitative phase restoration by direct inversion using the optical transfer function," *Opt. Lett.* **36**, 2671–2673 (2011).
6. D. Hamilton and C. Sheppard, "Differential phase contrast in scanning optical microscopy," *J. Microsc.* **133**, 27–39 (1984).
7. S. B. Mehta and C. J. Sheppard, "Quantitative phase-gradient imaging at high resolution with asymmetric illumination-based differential phase contrast," *Opt. Lett.* **34**, 1924–1926 (2009).
8. C. M. Vest, *Holographic Interferometry*, (John Wiley and Sons, Inc., 1979).
9. G. Popescu, *Quantitative Phase Imaging of Cells and Tissues* (McGraw-Hill, 2011).
10. B. Kachar, "Asymmetric illumination contrast: a method of image formation for video light microscopy," *Science* **227**, 766–768 (1985).
11. T. N. Ford, K. K. Chu, and J. Mertz, "Phase-gradient microscopy in thick tissue with oblique back-illumination," *Nat. Methods* **9**, 1195–1197 (2012).
12. L. Tian, J. Wang, and L. Waller, "3D differential phase-contrast microscopy with computational illumination using an LED array," *Opt. Lett.* **39**, 1326–1329 (2014).
13. D. Hamilton, C. Sheppard, and T. Wilson, "Improved imaging of phase gradients in scanning optical microscopy," *J. Microsc.* **135**, 275–286 (1984).
14. J. Mertz, A. Gasecka, A. Daradich, I. Davison, and D. Coté, "Phase-gradient contrast in thick tissue with a scanning microscope," *Biomed. Opt. Express* **5**, 407–416 (2014).
15. G. Zheng, C. Kolner, and C. Yang, "Microscopy refocusing and dark-field imaging by using a simple LED array," *Opt. Lett.* **36**, 3987–3989 (2011).

16. Z. Liu, L. Tian, S. Liu, and L. Waller, "Real-time brightfield, darkfield, and phase contrast imaging in a light-emitting diode array microscope," *J. Biomed. Opt.* **19**, 106002 (2014).
17. G. Zheng, R. Horstmeyer, and C. Yang, "Wide-field, high-resolution Fourier Ptychographic microscopy," *Nat. Photonics* **7**, 739–745 (2013).
18. L. Tian, X. Li, K. Ramchandran, and L. Waller, "Multiplexed coded illumination for Fourier Ptychography with an LED array microscope," *Biomed. Opt. Express* **5**, 2376–2389 (2014).
19. X. Ou, G. Zheng, and C. Yang, "Embedded pupil function recovery for Fourier ptychographic microscopy," *Opt. Express* **22**, 4960–4972 (2014).
20. L. Tian and L. Waller, "3D intensity and phase imaging from light field measurements in an LED array microscope," *Optica* **2**, 104–111 (2015).
21. N. Streibl, "Three-dimensional imaging by a microscope," *J. Opt. Soc. Am. A* **2**, 121–127 (1985).
22. H. Rose, "Nonstandard imaging methods in electron microscopy," *Ultramicroscopy* **2**, 251–267 (1977).
23. B. Hornberger, M. Feser, and C. Jacobsen, "Quantitative amplitude and phase contrast imaging in a scanning transmission x-ray microscope," *Ultramicroscopy* **107**, 644–655 (2007).
24. M. Born and E. Wolf, *Principles of Optics: Electromagnetic Theory of Propagation, Interference and Diffraction of Light* (Cambridge University Press, 1999).
25. H. Hopkins, "On the diffraction theory of optical images," *Proc. R. Soc. London, Ser. A* **217**, 408–432 (1953).
26. C. Sheppard and A. Choudhury, "Image formation in the scanning microscope," *J. Mod. Opt.* **24**, 1051–1073 (1977).
27. M. Bertero and P. Boccacci, *Introduction to Inverse Problems in Imaging* (Taylor & Francis, 1998).

1. Introduction

Phase imaging aims to recover a sample's optical path length (i.e. phase) from intensity measurements. At the sample plane, intensity images generally do not contain any phase information. However, *any* complex optical transfer function provides phase contrast, by which some of the sample's phase information is translated into measurable intensity variations. For example, Zernike phase contrast is achieved by introducing a phase delay of the zeroth order diffraction at the pupil plane [1]. Defocus is another convenient way to introduce tunable complex transfer functions [2–5]. In this paper, we analyze asymmetric illumination as a means for introducing phase contrast, and develop stable inversion methods which recover quantitative phase using differential phase contrast (DPC) [6, 7].

Quantitative phase imaging techniques usually require spatially coherent illumination (e.g. interferometry [8, 9]); in contrast, partially coherent methods such as DPC provide $2\times$ better lateral resolution limit, better optical sectioning, and reduction of speckle noise. Phase contrast can be achieved simply by using any asymmetric illumination pattern [10]. In DPC, quantitative phase is recovered from two images, taken with complementary asymmetric illumination patterns [7]. The difference between the two images is related to the sample's phase derivative along the axis of asymmetry. Conveniently, DPC only requires hardware changes on the illumination side [7, 11, 12] or on the detection side [6, 13, 14], thus it can be integrated into existing systems (e.g. endoscopy [11]).

Recently, we implemented DPC with an LED array microscope [12], which uses computational illumination for flexibly achieving a diverse array of imaging capabilities (e.g. dark-field [15, 16], phase contrast [12, 16], Fourier Ptychography [17, 18], digital aberration removal [19], light field refocusing [12, 15], and 3D phase imaging [20]). The hardware involves simply replacing a microscope's illumination unit with an LED array (Fig. 1). Each LED can be controlled individually to illuminate the sample from a unique angle. To implement DPC, we capture two images: one with a half circle of LEDs on, and one with the other half on. Because of the flexible patterning of the LED array, we are able to implement DPC measurements in real-time and along arbitrary axes of asymmetry, without any mechanical parts [12].

In this paper, we derive the weak object transfer function (WOTF) [13, 21] to quantify how phase information is converted into intensity in our DPC measurements, then develop quantitative inversion methods. The phase derivative model [6, 7] is only accurate in 1D and within the numerical aperture (NA) of the microscope objective [13, 22]. We derive here the full 2D

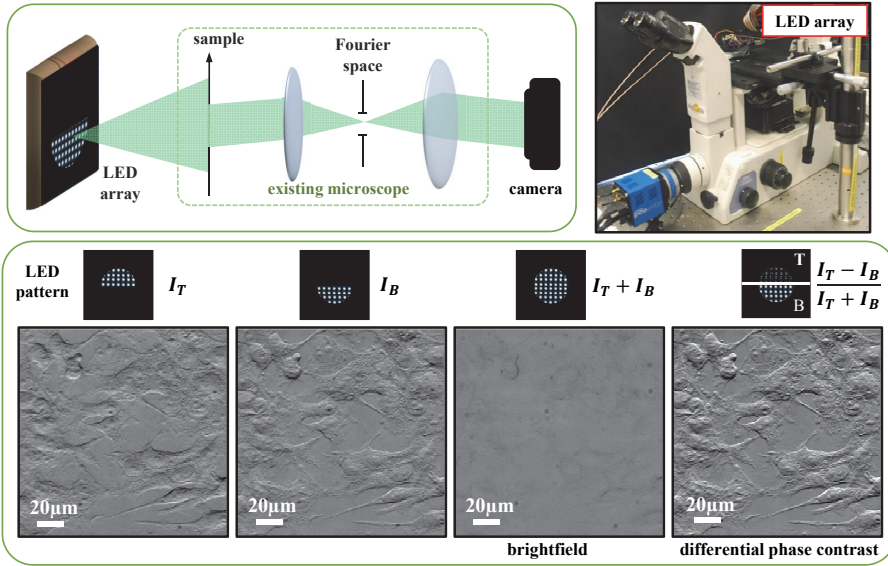


Fig. 1. Top: The LED array microscope places a programmable source sufficiently far from the sample to be in Fourier space. Bottom: Intensity images taken with the top and bottom halves of the LEDs on demonstrate strong phase contrast (HeLa cell, 20 \times 0.4 NA). The typical brightfield image (incoherence parameter = 1), is generated by the sum of the two half-circle images and contains no phase contrast. The differential phase contrast (DPC) image is the normalized difference of the two half-circle images.

model for all spatial frequencies out to the partially coherent bandlimit of the objective. We further model the discrete source distribution in our LED array setup to improve phase recovery for our system. The phase transfer function is anti-symmetric and zero at all spatial frequencies along the axis of asymmetry. These missing frequencies produce phase reconstruction artifacts, which we mitigate by using a regularized deconvolution method. To fully remove these artifacts, we capture additional DPC measurements along other axes to acquire the missing frequency information. The combined phase transfer function covers all spatial frequencies except for the origin (representing an arbitrary constant phase offset), and thus improves our phase reconstructions. Using the WOTF model, we study how phase contrast is affected by spatial coherence (source shapes). Reducing the source size results in poor phase contrast due to loss of low spatial frequency information and also narrower bandwidth in the transfer function. Using annular sources provides a convenient way to adjust the phase contrast by changing the inner radius, while maintaining the partially coherent bandwidth. This phase transfer function analysis and reconstruction technique may also find use in its application to alternative DPC architectures based on split-detectors [6, 13, 14, 23].

2. Theory and method

2.1. Phase transfer function for differential phase contrast

Consider a thin sample with complex transmission function $o(\mathbf{r}) = \exp[-\mu(\mathbf{r}) + i\phi(\mathbf{r})]$, where μ characterizes the sample's absorption and ϕ the phase, with $\mathbf{r} = (x, y)$ being the spatial coordinates. The field at the sample plane from illumination by a single point source is the product of the illumination $q(\mathbf{r})$ and sample's transmittance function $o(\mathbf{r})$. The field is then low pass filtered by the pupil function $P(\mathbf{u}'')$ (in the Fourier space) before reaching the camera (in the

real space), where \mathbf{u}'' denotes the coordinates at the pupil plane. The intensity at the camera due to a point source (coherent) illumination can thus be written as

$$I(\mathbf{r}_c) = \left| \iint \left[\iint q(\mathbf{r}) o(\mathbf{r}) \exp(-i2\pi\mathbf{r} \cdot \mathbf{u}'') d^2\mathbf{r} \right] P(\mathbf{u}'') \exp(-i2\pi\mathbf{u}'' \cdot \mathbf{r}_c) d^2\mathbf{u}'' \right|^2, \quad (1)$$

where \mathbf{r}_c denotes the coordinates at the camera plane. When the sample is illuminated by an extended incoherent primary source with intensity distribution $S(\mathbf{u}')$, where \mathbf{u}' denotes the scaled coordinates on the source plane, the intensity at the camera is then the incoherent sum of images due to each source point (neglecting magnifications and scaling factors) [24]:

$$I(\mathbf{r}_c) = \iint \left| \iint \left[\iint q(\mathbf{r}) o(\mathbf{r}) \exp(-i2\pi\mathbf{r} \cdot \mathbf{u}'') d^2\mathbf{r} \right] P(\mathbf{u}'') \exp(-i2\pi\mathbf{u}'' \cdot \mathbf{r}_c) d^2\mathbf{u}'' \right|^2 d^2\mathbf{u}'. \quad (2)$$

Since the LED array is placed sufficiently far away from the sample, the illumination from each LED is approximated by a plane wave at the sample, such that the overall illumination is

$$q(\mathbf{r}) = \sqrt{S(\mathbf{u}') \exp(i2\pi\mathbf{u}' \cdot \mathbf{r})}. \quad (3)$$

The phase contrast for asymmetric illumination comes from differential filtering in the pupil plane for each source position, such that asymmetry in Fourier space due to phase effects creates intensity in real space. In order to obtain a transfer function for phase contrast, we need to first group the source and pupil terms into a single transfer function, in order to incorporate illumination effects. This resulting system transfer function is known as either the 4D partially coherent transfer function or the transmission cross coefficient (TCC) model [25, 26]. Still, the relation between the measured intensity and the sample's absorption or phase is nonlinear.

We linearize the problem by adopting a weak object approximation, $o(\mathbf{r}) \approx 1 - \mu(\mathbf{r}) + i\phi(\mathbf{r})$ [13, 21, 22], and neglecting the cross terms from μ and ϕ , so that

$$o(\mathbf{r})o^*(\mathbf{r}') \approx 1 - [\mu(\mathbf{r}) + \mu(\mathbf{r}')] + i[\phi(\mathbf{r}) - \phi(\mathbf{r}')]. \quad (4)$$

By doing so, the intensity is separated into three terms: background term, absorption contrast term, and phase contrast term [21]. To further facilitate a transfer function analysis, we take the Fourier transform of both sides of Eq. (2) after substituting in Eqs. (3) and (4). The resulting intensity's spectrum, \tilde{I} , written as the sum of the three terms, is [13, 21]

$$\tilde{I}(\mathbf{u}) = B\delta(\mathbf{u}) + H_{\text{abs}}(\mathbf{u}) \cdot \tilde{\mu}(\mathbf{u}) + H_{\text{ph}}(\mathbf{u}) \cdot \tilde{\phi}(\mathbf{u}), \quad (5)$$

where $\tilde{\cdot}$ denotes Fourier transform, and $\mathbf{u} = (u_x, u_y)$ the spatial frequency coordinates.

The background term measures the total energy passing through the imaging system:

$$B = \iint S(\mathbf{u}') |P(\mathbf{u}')|^2 d^2\mathbf{u}'. \quad (6)$$

The benefit of making a weak object approximation is that the contrast due to absorption and phase are now decoupled and linear, so can be analyzed independently. The frequency response for absorption is characterized by the absorption transfer function,

$$H_{\text{abs}}(\mathbf{u}) = - \left[\iint S(\mathbf{u}') P^*(\mathbf{u}') P(\mathbf{u}' + \mathbf{u}) d^2\mathbf{u}' + \iint S(\mathbf{u}') P^*(\mathbf{u}') P(\mathbf{u}' - \mathbf{u}) d^2\mathbf{u}' \right], \quad (7)$$

and the frequency response for phase is characterized by the phase transfer function,

$$H_{\text{ph}}(\mathbf{u}) = i \left[\iint S(\mathbf{u}') P^*(\mathbf{u}') P(\mathbf{u}' + \mathbf{u}) d^2\mathbf{u}' - \iint S(\mathbf{u}') P^*(\mathbf{u}') P(\mathbf{u}' - \mathbf{u}) d^2\mathbf{u}' \right]. \quad (8)$$

The WOTFs in Eqs. (7) and (8) are general and can be applied to any source and pupil functions. To derive the specific transfer functions for DPC, we must consider taking two images to compute the phase contrast image, I^{DPC} [6, 7]:

$$I^{\text{DPC}}(\mathbf{r}_c) = \frac{I_T(\mathbf{r}_c) - I_B(\mathbf{r}_c)}{I_T(\mathbf{r}_c) + I_B(\mathbf{r}_c)}, \quad (9)$$

where I_T and I_B represent the top and bottom measurements, taken with uniformly distributed incoherent sources of half-circle shape (Fig. 1). The radius of the circle determines the NA of the illumination, NA_{illum} , which is usually set to match the NA of the objective, NA_{obj} . Thus, the effective source for DPC measurements is anti-symmetric and the background term is canceled after the subtraction. As a result, the DPC image has better phase contrast than single-side asymmetric illumination. More importantly, it can be used to quantitatively recover phase.

For an aberration-free system, the pupil function is a (real and symmetric) circular function, whose radius is set by the NA of the objective. In this case, the absorption transfer function is

$$H_{\text{abs}}^{\text{DPC}}(\mathbf{u}) = 0, \quad (10)$$

meaning that an ideal DPC image does not contain any absorption information. Note that both aberrations and defocus can introduce unwanted absorption contrast to the DPC image [13].

The phase transfer function $H_{\text{ph}}^{\text{DPC}}(\mathbf{u})$, shown in Fig. 2, is anti-symmetric, with zeros along the axis of asymmetry. The bandwidth of the system is twice that allowed by the objective NA, due to partially coherent illumination. Within the NA of the objective, the transfer function is similar to the first derivative model. However, since the source and pupil affect Eq. (8) in a cross-correlation manner, higher frequencies will be damped. Thus, the two transfer functions deviate significantly at high frequencies. Further, we note that the original theory for DPC assumes a continuous half-circle source shape, while our LED array has 32×32 LEDs arranged in a discrete grid pattern. We account for this by treating each LED as a coherent point source, which causes stair-case like discrete jumps in the transfer function.

The Fourier spectrum of the DPC image can then be modeled as

$$\tilde{I}^{\text{DPC}}(\mathbf{u}) = H(\mathbf{u}) \cdot \tilde{\phi}(\mathbf{u}), \quad (11)$$

where $H(\mathbf{u}) = H_{\text{ph}}(\mathbf{u})/B$ and the sum of the two images corresponding to the brightfield image is approximated by B . We will use this transfer function to solve the phase retrieval inverse problem, giving more accurate results than is given by the usual first derivative approximation.

2.2. Quantitative phase reconstruction method

Quantitative phase can be recovered by deconvolving the DPC image using the calculated transfer function. Since $H(\mathbf{u})$ is zero at frequencies along the axis of asymmetry and beyond the passband, direct deconvolution will dramatically amplify the noise present at these frequencies, giving poor results. Here, we solve the following least-squares problem

$$\min \sum_j |\tilde{I}_{\text{DPC},j}(\mathbf{u}) - H_j(\mathbf{u}) \cdot \tilde{\phi}(\mathbf{u})|^2 + \alpha |\tilde{\phi}(\mathbf{u})|^2, \quad (12)$$

where j is the index of DPC measurements (e.g. to account for the multi-axis DPC case) and α is a regularization parameter. The solution is equivalent to Tikhonov regularization [27]:

$$\phi_{\text{tik}}(\mathbf{r}) = \mathcal{F}^{-1} \left\{ \frac{\sum_j H_j^*(\mathbf{u}) \cdot \tilde{I}_{\text{DPC},j}(\mathbf{u})}{\sum_j |H_j(\mathbf{u})|^2 + \alpha} \right\}, \quad (13)$$

where $\mathcal{F}^{-1}\{\cdot\}$ denotes inverse Fourier transform.

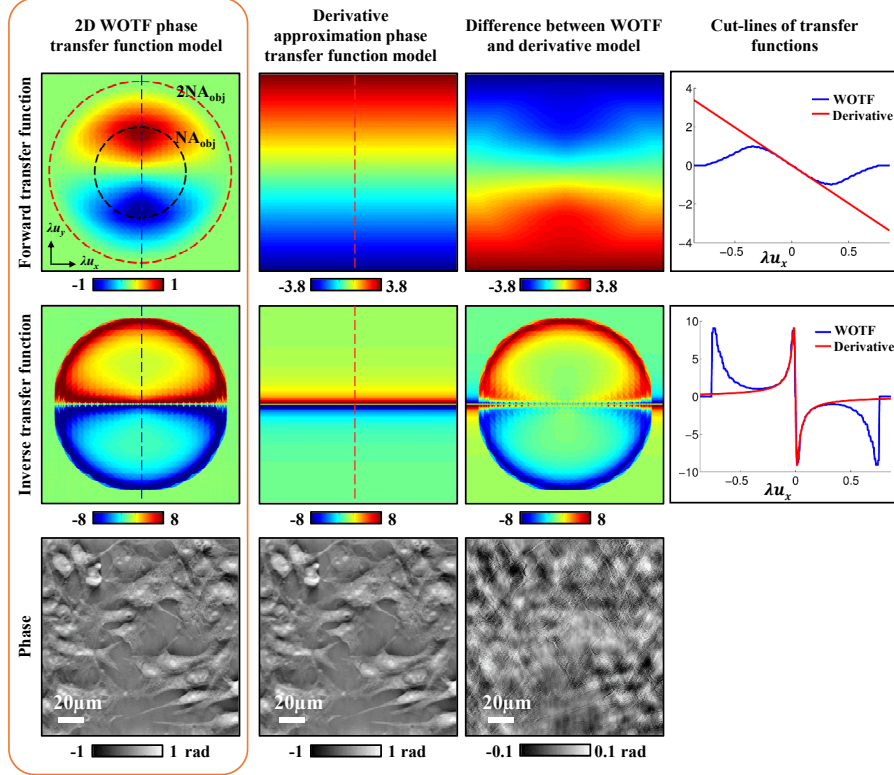


Fig. 2. The 2D WOTF phase transfer function of DPC does not exactly match the first derivative approximation that is generally used. Here we compare transfer functions from WOTF model (Column 1) with the derivative model (Column 2). Both recover spatial frequencies out to twice the NA of the objective (black and red dashed circles are spatial frequencies NA/λ and $2NA/\lambda$, respectively). However, our inverse transfer function compensates for damping of high frequencies, so small details are better recovered. Quantitative phase (Row 3) is reconstructed using data from Fig. 1 with regularization ($\alpha = 10^{-3}$).

In Fig. 2, we compare the inverse transfer functions for single-axis DPC reconstruction

$$H_{\text{tik}}(\mathbf{u}) = H_0^*(\mathbf{u}) / (|H_0(\mathbf{u})|^2 + \alpha), \quad (14)$$

where $H_0(\mathbf{u}) = H(\mathbf{u})$ for our model, and $H_0(\mathbf{u}) = i\beta u_x$ for the derivative model (the slope β depends on illumination and objective NAs). Our 2D WOTF inverse model compensates for the reduced contrast at high frequencies due to partially coherent illumination, whereas the derivative approximation inverse model acts as a low pass filter, attenuating the high frequency phase information and partially blurring fine details of the phase result.

3. Experimental results

Our experimental setup (Fig. 1) consists of a 32×32 custom-made LED array (4mm spacing, central wavelength 513nm with 20nm bandwidth) placed 63mm above the sample, replacing the microscope's standard illumination unit (Nikon TE300 inverted). The LED array is controlled by an ARM microcontroller and synchronized with the camera (PCO.edge) to switch the LED patterns at 40Hz while capturing full-frame (2160×2560) 16 bit videos. Thus, we can capture single-axis DPC measurements at 20Hz, though we usually implement 2-axis DPC

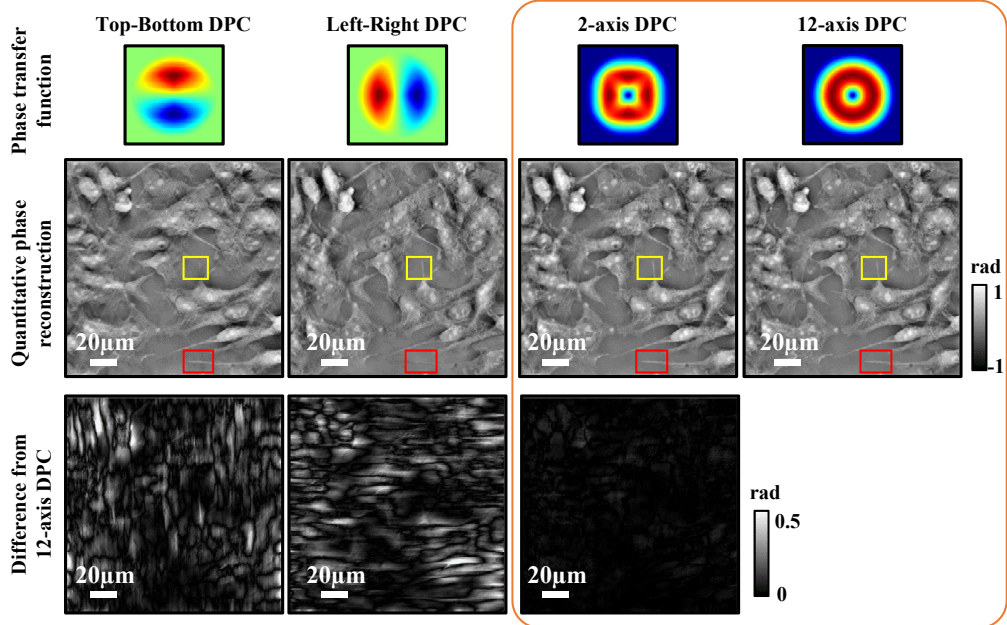


Fig. 3. Multi-axis DPC phase reconstructions (HeLa cells) eliminate artifacts due to missing frequencies along the axis of asymmetry. (Left) Single-axis DPC with Top-Bottom source asymmetry results in missing vertical features (yellow boxes), while Left-Right source asymmetry results in missing horizontal features (red boxes). (Right) Combining 2-axis or 12-axis data results in improved phase recovery, due to better coverage of spatial frequencies. As more angles are added, up to 12, the transfer function changes only marginally. (Bottom row) The 12-axis phase result is used as a best estimate of true phase, in order to show the errors incurred when using fewer angles.

for better phase reconstruction fidelity. Example images are all taken with a 20×0.4 NA objective. Illumination from each LED is approximately spherical in our setup, resulting in small intensity inhomogeneities across the field of view that are not accounted for by the plane wave model. To correct for this, we calibrate the background by taking DPC measurements without any sample in place. Each sample's image is then divided by the corresponding background image before calculating the DPC image (as in Fig. 1).

3.1. Single and multi-axis DPC

Our 2D WOTF phase transfer function model provides significant improvement for recovering high frequency features as compared to the simple derivative model. Still, phase reconstructions from a single-axis of asymmetry are fundamentally limited by the missing frequencies along the axis of asymmetry. For example, in the two right-hand columns of Fig. 3, the yellow and red boxes highlight vertical and horizontal features, respectively, that are not well reconstructed when they align with the direction of asymmetry. Combining DPC measurements along two different axes eliminates the missing frequencies and thus improves the phase reconstruction. Given that our reconstruction algorithm is general for any number of directions of DPC measurements, it is straightforward to extend the transfer function calculation to two or more angles of DPC measurements and then deconvolve to recover phase using Eq. (13). As demonstrated in Fig. 3, the combined phase transfer function (visualized by $\sqrt{\sum_j |H_j(\mathbf{u})|^2}$) from two DPC measurements along orthogonal axes is zero only at the origin and outside the passband.

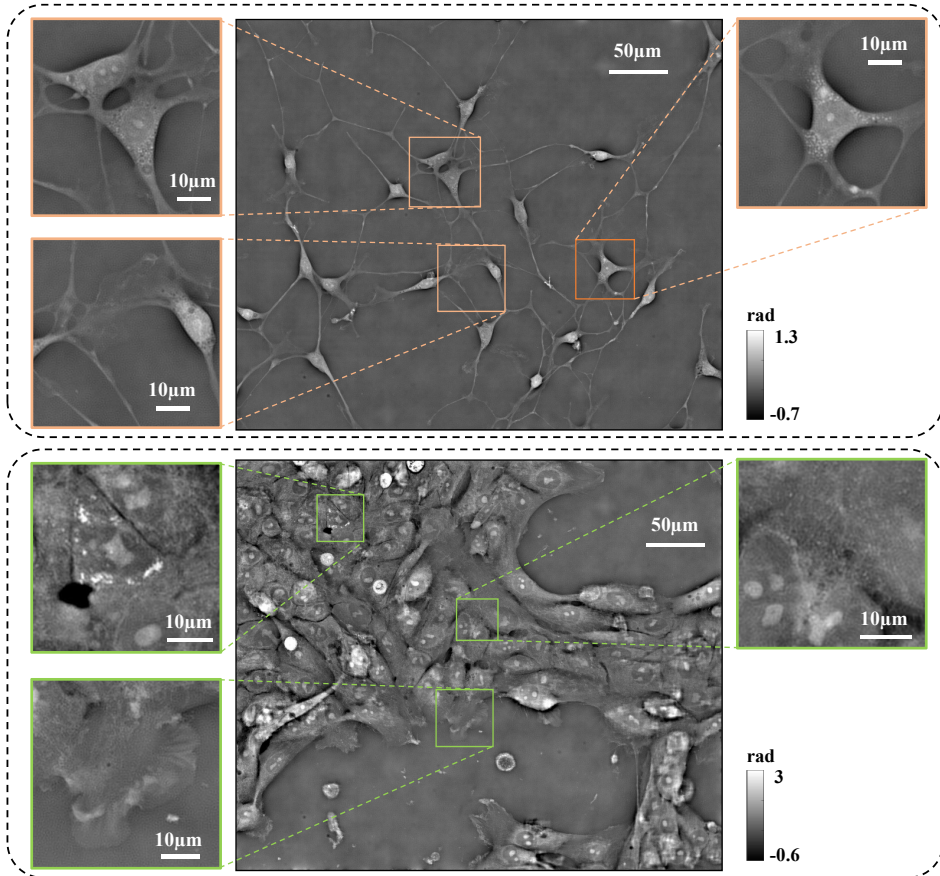


Fig. 4. Quantitative phase imaging at 10 Hz with 0.8 NA. The 2-axis DPC images are taken with a 20×0.4 NA objective by repeating top, bottom, left and right half-circle illumination at 40Hz. Real-time sub-cellular dynamics can be visualized in the accompanying videos for both (Top) unstained neural progenitor cells (NPC) after five days of differentiation ([Media 1](#)), and (Bottom) unstained MCF10A human breast basal epithelial cell ([Media 2](#)).

The phase reconstruction using our regularized deconvolution method largely removes the artifacts which are present in the single-axis DPC reconstructions. Since our LED array microscope is capable of implementing DPC at many different angles of asymmetry, we can further examine the improvement achieved by using many angles of DPC measurements. The combined phase transfer function for 12 equally spaced DPC measurements (i.e. at every 15°) is shown in Fig. 3 (right-most column) to be almost circularly symmetric, providing only slight improvement over the 2-axis result. As a result, we conclude that DPC measurements from two orthogonal axes provide the best trade-off between phase reconstruction accuracy and acquisition speed.

To demonstrate real-time quantitative phase imaging capability, we image unstained live neural progenitor cells and human breast basal epithelial cells by implementing 2-axis DPC. The raw data is captured at 40Hz by sequentially scanning through the 4 illumination patterns (top, bottom, left, right half circles) in a continuous loop. Thus, the end result is quantitative phase at 10Hz. The images are taken with a 20×0.4 NA objective, providing $0.33\mu\text{m}$ resolution in the phase reconstruction (0.8 effective NA). Sub-cellular dynamics, such as movements of vesicles, can be clearly observed, as shown in Fig. 4 and its accompanying videos.

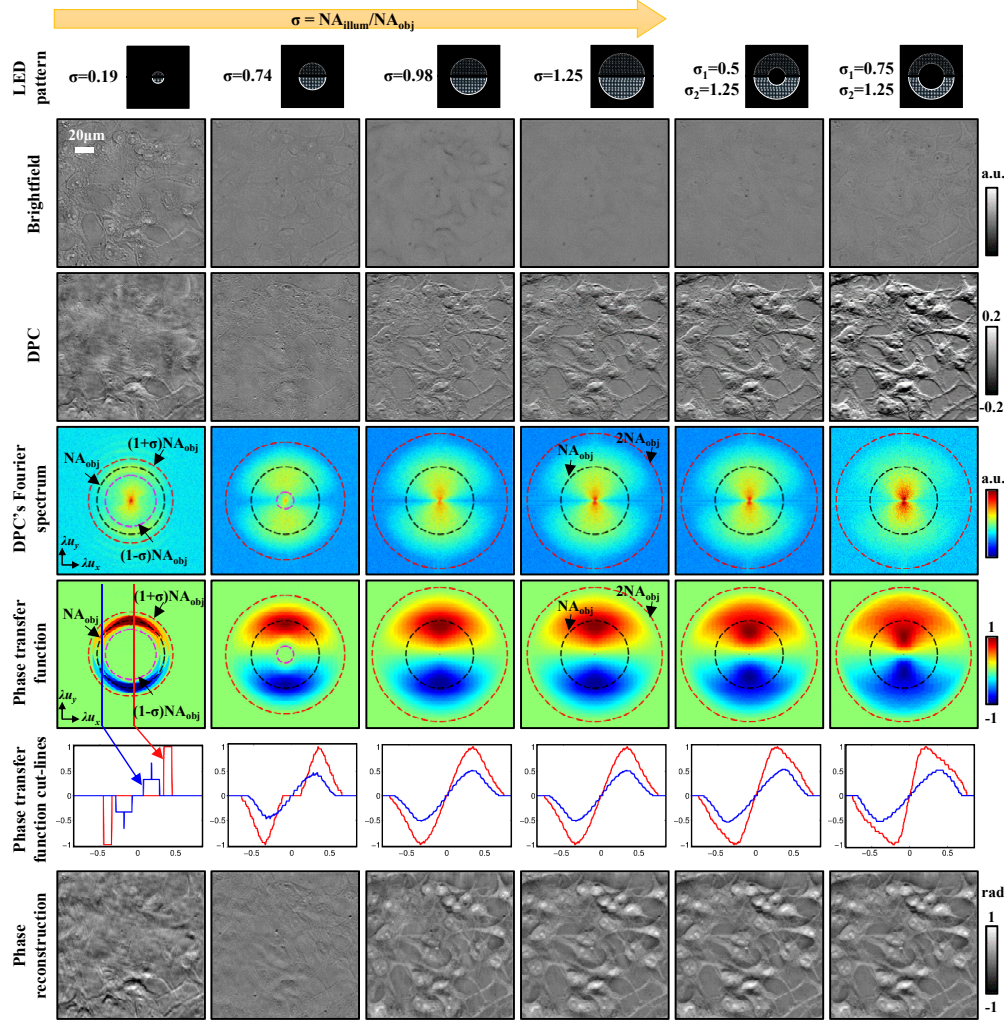


Fig. 5. DPC requires illumination from high angles for good phase recovery at all spatial frequencies. As the illumination NA increases (measured by the coherence parameter σ), both low spatial frequency and high spatial frequency phase information are better captured. When we use a half-circle source with $\sigma \leq 1$, spatial frequencies below $(1 - \sigma)NA_{\text{obj}}/\lambda$ and above $(1 + \sigma)NA_{\text{obj}}/\lambda$ are missing. Thus, DPC only achieves resolution corresponding to twice the NA of the objective when $\sigma \geq 1$. Interestingly, DPC with half-annular sources provides improved contrast for low spatial frequencies, maintaining the maximum 2NA bandlimit without sacrificing high spatial frequency response.

3.2. Effect of spatial coherence of illumination

The phase transfer function can be tuned by using different illumination patterns according to Eq. (8), though DPC is usually implemented with half-circle illumination shapes. In Fig. 5, we study the effect of illumination NA by taking DPC measurements with gradually increasing coherence parameter $\sigma = NA_{\text{illum}}/NA_{\text{obj}}$, achieved by choosing the radius of the half-circle of LEDs to turn on accordingly. The DPC image taken with the most coherent illumination ($\sigma = 0.19$) contains significant artifacts due to coherent scattering from out-of-plane objects that results from poor depth sectioning. Further, these measurements are missing both high

and low spatial frequency information, resulting in poor Fourier space coverage and loss of the most important features in the recovered phase. Increasing σ reduces the coherent artifacts and improves the depth sectioning, while also allowing recovery of a wider range of spatial frequencies. The DPC image taken with $\sigma = 0.74$ provide good contrast for edge features (e.g. boundaries of cells), but is missing information from slowly varying features.

These observations match well with our phase transfer function theory, which predicts missing low-frequency information within $(1 - \sigma)\text{NA}_{\text{obj}}/\lambda$. The highest spatial frequency allowed is $(1 + \sigma)\text{NA}_{\text{obj}}/\lambda$, as shown by the Fourier spectrum of the DPC image in Fig. 5. The DPC image taken with $\sigma = 0.98$ still shows slightly lower contrast as compared to those taken with $\sigma \geq 1$, due to slight loss of low frequency information, which is extremely important for high-quality phase reconstruction. The remaining low frequency content in these DPC measurements may be due to imperfect modeling of the illumination from the LEDs. Further increasing the illumination NA to $\sigma = 1.25$ provides Fourier coverage up to twice the NA of the objective with little change to the transfer function shape.

An implication of our phase transfer function analysis is that we only need high angle illumination (outermost LEDs) to capture phase contrast for both low spatial frequency and high spatial frequency features. Thus, we may achieve good phase reconstruction not with a half-circle shape, but rather with a half-annulus shaped illumination, as long as the outer ring has $\sigma \geq 1$ and inner ring has $\sigma \leq 1$. The DPC measurements taken with two different half-annulus illumination patterns are shown in the right columns of Fig. 5. With a larger inner radius, the contrast of the DPC image is enhanced. This is because the linear region of the phase transfer function becomes steeper as the inner radius is increased, giving better contrast for low-frequency features. Importantly, the high frequency information is still well captured with a slightly lower contrast as compared to the half-circle case. Thus, the annular DPC measurement provides a convenient way to tune the phase transfer function for better measuring and recovering the spatial frequency region of interest.

4. Conclusion

We have presented a 2D transfer function analysis and quantitative phase reconstruction method for differential phase contrast using partially coherent asymmetric illumination. Images are captured in an LED array microscope, which is particularly attractive for commercial microscopy, since it can achieve illumination pattern switching at camera-limited speed. We demonstrate phase imaging at 10Hz with $0.33\mu\text{m}$ (0.8 NA) resolution, showing videos of sub-cellular dynamics. The method is label-free and stain-free, so has application in imaging live samples.

Acknowledgments

The authors thank Ziji Liu and Jingshan Zhong for help with experiments, Rene Claus for helpful discussions, and Peiwu Qin and Olivia Scheideler for providing samples. Funding was provided by the Gordon and Betty Moore Foundation's Data-Driven Discovery Initiative through Grant GBMF4562 to Laura Waller.